# Multi-scale simulation and finite-element-assisted computation of elastic properties of braided textile reinforced composites

Ji, Xianbai; Khatri, Aditya M; Chia, Elvin SM; Cha, Ryan KH; Yeo, Bern TB; Joshi, Sunil C; Chen, Zhong

2013

Ji, X., Khatri, A. M., Chia, E. S., Cha, R. K., Yeo, B. T., Joshi, S. C., et al. (2014). Multi-scale simulation and finite-element-assisted computation of elastic properties of braided textile reinforced composites. Journal of composite materials, 48(8), 931-949.

https://hdl.handle.net/10356/102895

https://doi.org/10.1177/0021998313480198

# Multi-scale Simulation and FE-Assisted Computation of Elastic Properties of Braided Textile Reinforced Composites

Xianbai Ji[a], Aditya M. Khatri[a], Elvin S.M. Chia[b], Ryan K.H. Cha[c], Bern T.B. Yeo[d], Sunil C. Joshi[e*], Zhong Chen[e*]

[a] Temasek Laboratories@NTU, 50 Nanyang Drive, Singapore 637553

[b] DSO National Laboratories, 20 Science Park Drive, Singapore 118230

[c] Singapore Technologies Kinetics Ltd, 249 Jalan Boon Lay, Singapore 619523

[d] Temasek Polytechnic, 21 Tampines Avenue 1, Singapore 529757

[e] Nanyang Technological University, 50 Nanyang Avenue, Singapore 639798

## ABSTRACT

This paper deals with computation of effective elastic properties of braided textile composites assisted by finite element analysis (FEA). In this approach, dynamic representative unit cells are first constructed to model typical geometry of braided textile preform. Subsequently, after establishing the elastic properties of braiding yarns, the effective Young's moduli, shear moduli and Poisson's ratios corresponding to varying braiding angles are obtained by analysing these geometric models of preform with the help of the commercial FEA code Abaqus. Effects of fibre volume fraction on the elastic properties of both biaxial and triaxial composite unit cells are also examined. Finally, bending behaviour of a simply supported beam with braided composite skin is evaluated via the FEA assisted multi-scale modelling, which is further verified experimentally. The predicted results compared favourably with the experiment, backing the accuracy of the proposed modelling approach.

KEYWORDS: textiles, mechanical properties, FEA, braiding, multi-scale simulation.

* Corresponding authors. Tel: +65 6790 4256 Email: ASZChen@ntu.edu.sg (Z. Chen) & Tel: +65 6790 5954 Email: MSCJoshi@ntu.edu.sg (S.C. Joshi)

# BIOGRAPHIES OF AUTHORS

**Xianbai Ji**

Xianbai is currently a researcher at Temasek Laboratories@NTU, Singapore. He received his Bachelor's degree in Materials Science and Engineering from Xiamen University, China. He carried out his final year project in NTU under the Temasek Foundation - Nanyang Technological University Leadership Enrichment and Regional Networking Scholarship (TF-NTU LEaRN) on the synthesis and characterisation of photocatalyst materials. His research interests mainly include mechanics of materials, finite element analysis, solid modelling and materials structure. He is also a reviewer of an Elsevier journal. Besides the academic research, he was involved in various policy debates on ASEAN and formed a part of a Southeast Asia delegation to the European Union in 2012.

**Aditya M. Khatri**

Aditya M. Khatri obtained his Bachelor's degree in Aerospace Engineering with Double Minors in Economics and Computing from Nanyang Technological University, Singapore in 2009. He is currently working on his Masters degree in aerospace composites. This research work was done during his employment at Temasek Laboratories@NTU from 2009-2012. His research interests cover various aerospace fields. He was the conceptual satellite power systems engineer for the Ship Tracking and Environmental Protection Satellite preliminary design project under DSO National Laboratories in 2006 and the Deployable Space Structures satellite deployable antenna designer under DSO / DSTA Undergraduate REsearch on CAmpus (URECA) in 2007. He also worked in the field of Computational Fluid Dynamics (CFD) investigating unsteady flow fields and trajectories of moving bodies.

**Elvin S.M. Chia**

Chia Ser Ming, Elvin obtained his B.Eng (Hons) in Mechanical Engineering from the National University of Singapore in 1993. He then joined DSO National Laboratories of Singapore as a research engineer and has been with the company till present. He was a visiting research scholar at the Center of Composite Materials (CCM) of the University of Delaware in 1999-2000; and at the Fibrous Materials Research Center (FMRC) of the Drexel University in 2001-2002. He was conferred the title of Principal Member of Technical Staff specialising in composites research and development in 2011. His current research interests are in the areas of composite fabrication techniques (vacuum bagging, prepreg/autoclave, filament winding), resin infusion processes (e.g. VARI, RTM, RIRM), net-shape preforming technique (2-D and 3-D braiding) and multi-functional composites.

**Ryan K.H. Cha**

Cha Khoon Hock, Ryan graduated from the Singapore Polytechnic in 2003 and obtained his B.Eng (Hons) in Mechanical & Manufacturing Engineering from South University of Australia in 2009. He then worked as an Engineer in ST Kinetics from 2009 and has been with the company till present. His research and development works on composites have been focused on design and analysis of composites; producing prototype demonstrators and delivering composite products through exploiting a combination of manufacturing technologies which include prepreg/autoclaving, hand-layup, net-shape 2D braided preforming, and a variance of liquid infusion processes (VARI, VARTM, RTM).

**Bern T.B. Yeo**

Yeo Teck Boon, Bern graduated from the Singapore Polytechnic in 1992 with a Diploma in Mechanical Engineering. He then worked as an Associate Engineer in DSO National Laboratories from 1995 till 2011. His research interests were in the characterisation of composite materials and structures, specialise in the various testing techniques in the evaluation of composites to meet application requirements. He is presently with the Temasek Polytechnic as an Aviation Instructor.

**Sunil C. Joshi**

Dr. Sunil C. Joshi is currently a faculty in Aerospace Engineering Division of the School of Mechanical and Aerospace Engineering at Nanyang Technological University, Singapore. He received his doctorate from Monash University, Australia, for his work on simulation of composites manufacturing processes. His research interests and previous work encompass satellite thermal management, numerical simulation and optimization of composites manufacturing processes, development of specialty composite material systems, and curing and repair of composites. He was the team leader for thermal controls subsystem for the first microsatellite program in Singapore. Besides being actively involved in various research projects and administrative committees, he is an area editor of an Elsevier journal. To date he has more than 90 research publications to his credit.

**Zhong Chen**

Dr. Zhong Chen is currently a faculty member in the School of Materials Science and Engineering at Nanyang Technological University, Singapore. He has more than 20 years' research experience in the area of mechanical behaviour of materials, which includes mechanics and fracture mechanics of bulk, composite and thin film materials, materials joining, experimental and computational mechanics of materials. His other interests include energy and microelectronic materials. Zhong Chen currently serves as an editor / editorial board member for 5 international journals. He has also served as a reviewer for more than 50 academic journals and a number of research funding agencies including European Research Council (ERC). Zhong Chen is an author of 3 book chapters and more than 140 peer-reviewed journal articles.

## INTRODUCTION

Braiding is a traditional process of intertwining strands of fibres into textiles. The principal feature of braided textiles is the flexibility to form a wide range of geometric shapes in a cost-effective way [1]. Because of the preceding decades' efforts in making structural components lighter, stronger and tougher with increased bending strength, impact resistance, chemical immunity and torsional integrity, braided textile composites are being increasingly utilised in defence, aerospace, transportation, energy and sports industries.  Recently, dry carbon fibres composites have been applied favourably to the watch-making industry [2].

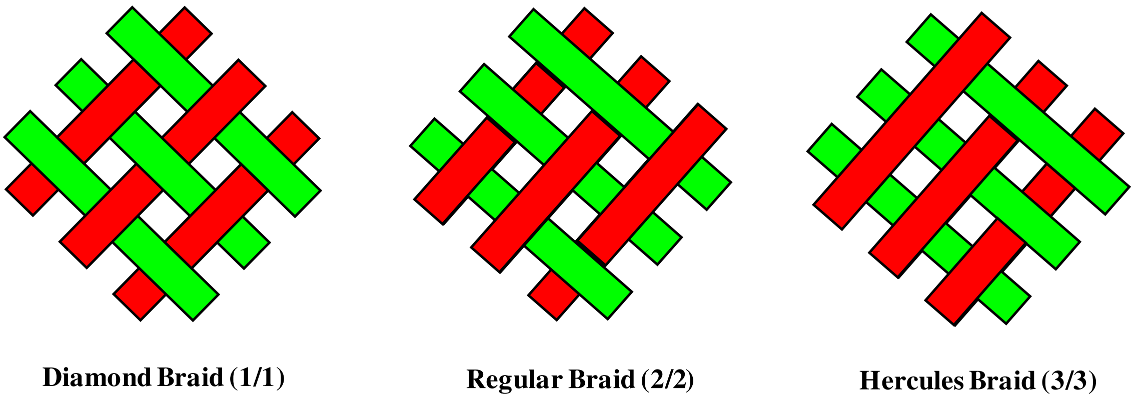


*Figure 1.Basic biaxial braid patterns*

There are two types of two-dimensional (2D) braids, the biaxial and the triaxial. The biaxial braid is comprised of two sets of bias yarns intertwining at an angle of 2θ. The angle θ is defined as the braiding angle, the single most critical parameters of braided structure. Depending on the braiding pattern, braids are distinguished as diamond braid (1 by 1), regular braid (2 by 2) and Hercules braid (3 by 3) as shown in Figure 1.  The diamond braid has a repetition of one yarn passing under and then over another yarn; the yarns in a regular braid pass below two and above two other yarns alternatively and the Hercules braid is characterised by a three below and three above interlacing pattern. The triaxial braid has an additional set of axial yarns inserted equiangular between +θ and −θ bias braiding yarns.

To take advantage of the unique features braided textiles and their composites could offer, extensive research has been carried out to study the mechanical properties of braided textile composites both analytically and experimentally. Naik and Shembekar [3] presented a 2D model for the elastic analysis of a plain weave fabric lamina and compared the elastic moduli predicted by different analytical models. Quek et al. [4] developed an analytical model for the calculation of the effective elasticity of 2D triaxial braided composite and studied the effect of initial micro-imperfections. Based on the principle of superposition, Miravete et al. [5] formulated an analytical mesomechanical model to predict the properties of braided composites. Falzon and Herszberg [6] and Dauda et al. [7] conducted tension, compression and shear tests on braided composites to characterise their properties. Littell et al. [8] adopted optical measurement techniques to overcome the limitations of strain gauge and correlated the local and the global deformations of braided composite under tension. Masters et al. [9] investigated the mechanical properties of triaxial braided textile composites by both experimental and analytical methods, highlighting the significance of the textile preform architecture in determining the composite behaviour.

Despite being preferred in many cases, the traditional analytical and experimental approach lacks the capability to depict the stress and strain distribution throughout the braided structure. Many researchers instead implemented finite element analysis (FEA) to investigate braided textile composites in recent years. Tsai et al. [10] used a parallelogram spring model to predict the effective elastic properties of 2D braided composites in which yarns were modelled by one-dimensional spring element. Xu et al. [11] predicted the properties of braided textile composites by three-dimensional (3D) representative unit cells. Goyal and Whitcomb [12] analysed the stress concentration within a tow for regular braided textile composites. Pickett et al. [13] systemically simulated the geometries of braiding yarns and braided textiles and a typical braiding process with explicit finite element techniques. However, few attempts have been reported on the 3D FE models of braided textile composites taking into account the effect of braiding process on the architecture of the textile reinforcement and its influences on the mechanical properties of the composite products.

The main objective of this paper is to build a reliable and versatile FE description of the textile hierarchy of structures within which the braiding parameters are reflected, and the change in properties is captured at different length scales. Subsequently, computer simulation can be used to design and optimize a structure or components made of braided composites based on the predicted mechanical and other responses. In this paper, biaxial and triaxial regular braids (2 by 2) are studied to predict the effective elastic properties for varying braiding angles, from 20° to 55° at an increment of 5°. The relation between the elastic constants and fibre volume fraction ($V_f$) is examined at the braiding angle of 60°. The verification of simulation results is generally conducted through experiments on coupons. However, as pointed out by Littell et al. [8], the tests on a small specimen may not truly reflect the actual composite behaviour because a number of the bias braiding yarns in the strain gauge section are not gripped by the fixture. Therefore, a uniquely designed experiment is adopted for direct comparison between a braided composite beam and its FE simulation results to verify the overall accuracy. This correlation is achieved through a multi-scale modelling strategy which follows three levels of analysis (see Figure 2) that links the properties of constituent materials to unit cell level properties, and these to the structural level mechanical behaviour. The micro-level analysis first involves determining the properties of matrix-infused yarns from the fibre properties using analytical methods. At the meso-level, elastic mechanical properties of the composite unit cells are obtained by FEA. The third level of analysis involves replacing the different braided regions within a structural component with homogenized elastic properties predicted by the unit cell outputs. Thus built, this entire structure subjected to loads then undergoes FEA simulation to predict its elastic responses.

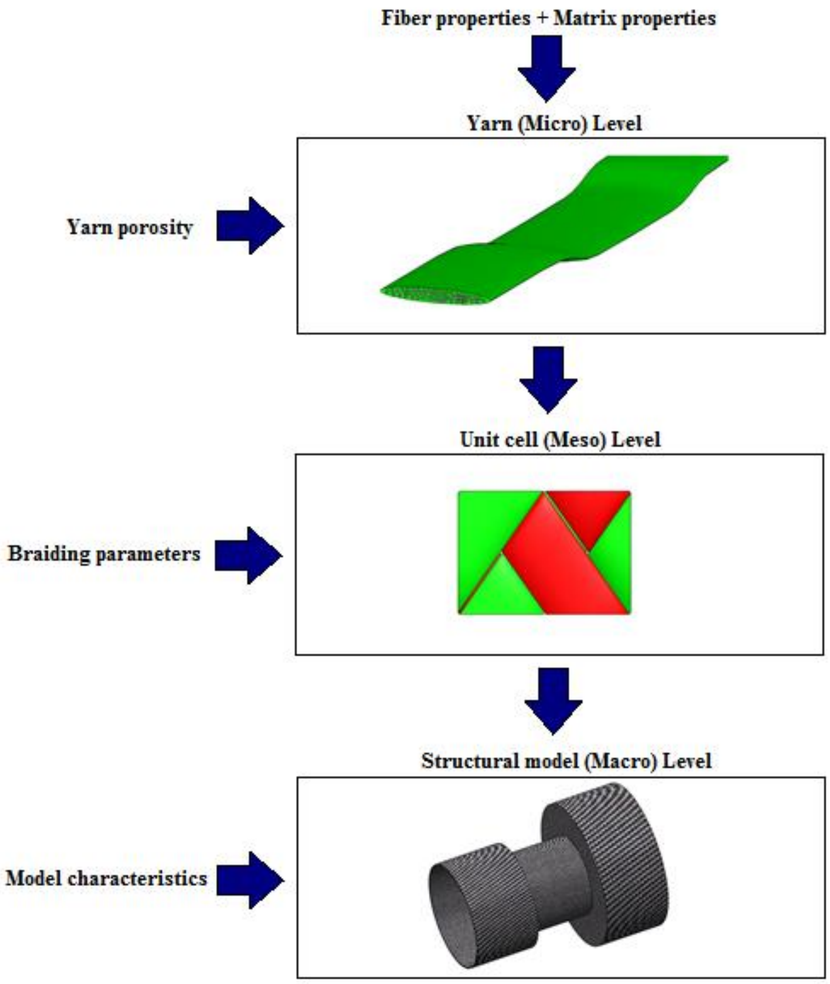


*Figure 2.Geometric hierarchy of the multi-scale modelling approach*

## GEOMETRIC MODELLING OF BRAIDED TEXTILE PREFORM AND COMPOSITE UNIT CELLS

A braided textile preform consists of interlaced +θ and −θ bias yarns in a biaxial braid and an additional axial yarn set in a triaxial braid. In creating unit cells using computer aided design (CAD) software, these components are modelled separately. Bias yarns are created by sweeping a cross section with an elliptical shape along a predefined undulation path. In a typical braiding process, the axial yarns are laid first with equal distance and bias yarns deposit on them subsequently. In the triaxial models developed in this study, the axial yarn is assumed to be perfectly straight and is modelled by extruding an ellipse along a straight line. Then the bias and axial yarns are assembled together, according to certain braiding angle and spacing, to form a braided structure. From a careful observation of the complex braided textile, a smaller repeating unit can be identified. Figure 3 shows a regular triaxial braid unit cell in diamond shape and the geometric parameters, including braiding angle θ, dimension of braiding yarns $w_a$, $w_b$, $t_a$, $t_b$, and the gap between neighbouring yarns $\varepsilon$, that used to describe it.

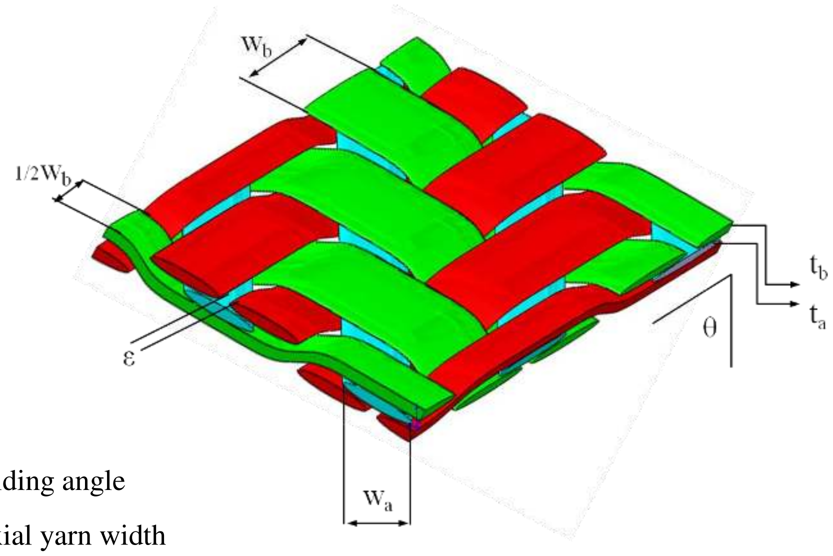


θ – Braiding angle

$w_a$ – Axial yarn width

$w_b$ – Bias yarn width

$t_a$ – Axial yarn thickness

$t_b$ – Bias yarn thickness

ε – Gap between neighbouring bias yarns

*Figure 3.Geometric parameters of a regular triaxial braid in diamond shape*

In order to internalise the effect of the braiding machine parameters, the relation of the unit cell parameters is governed by the Equation below [14]:

$$w_b + \varepsilon = \frac{2\pi D}{N_b}\cos\theta \qquad (1)$$

where $D$ is the part diameter (approximately equal to the diameter of the mandrel if the braid is very thin), and $N_b$ is the number of bias yarn carriers in the track plate of the braiding machine. Alternatively, a more flexible model is developed where the user can manually define the value of the aforementioned geometric parameters. These unit cells are used when the manufacturing conditions and information of the braiding process are unknown. Unit cells presented are dynamic in nature, exhibiting better flexibility as compared to the work by Xu et al. [11] which only takes the tightest configuration into account.

In terms of solid modelling construction, the unit cell yarn consists of an ellipse-shaped profile that is swept through a defined path to create the yarn volume. The yarn profile geometry is an ellipse defined by the bias yarn thickness, $t_b$ and bias yarn width, $w_b$. The yarn path geometry is defined such that it will wind around the neighbouring bias yarns, and is thus indirectly affected by the surrounding yarns' geometry as shown in Figure 4.

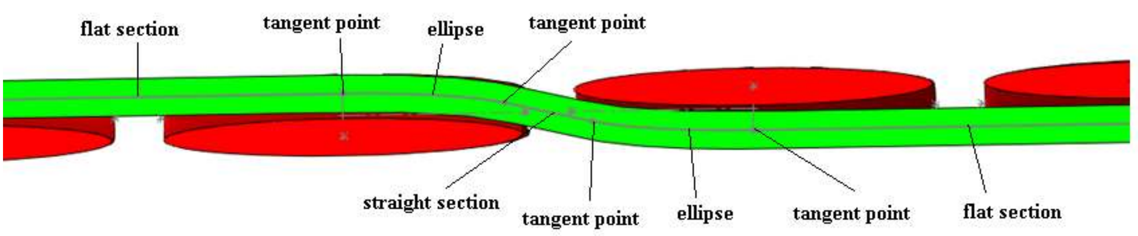


*Figure 4.The part ellipses and geometry features used to create the yarn path*

The bias yarn path is seen to wind around the neighbouring bias yarns such that the final swept yarn volume will not intermix with the surrounding bias yarn volumes. As shown in Figure 4, the yarn path consists of flat sections and knee sections (where the yarns transition from below-to-above or vice versa). The knee section itself consists of part ellipses connected tangentially by straight segments. The shape of these part ellipses take into account the widths and thicknesses of the surrounding yarns; whereas, the length of the part ellipses and the segment is determined automatically by the solid modelling software such that all points of the yarn path and tangential.

To facilitate the subsequent FEA, the diamond braided textile unit cell is further cut into a smaller repeatable unit cell in rectangular shape. Discussed firstly by Sun et al. [15], a reasoning Boolean operation based heterogeneous CAD modelling technique is used to convert a braided textile preform to a braided textile composite unit cell as shown in Figure 5.

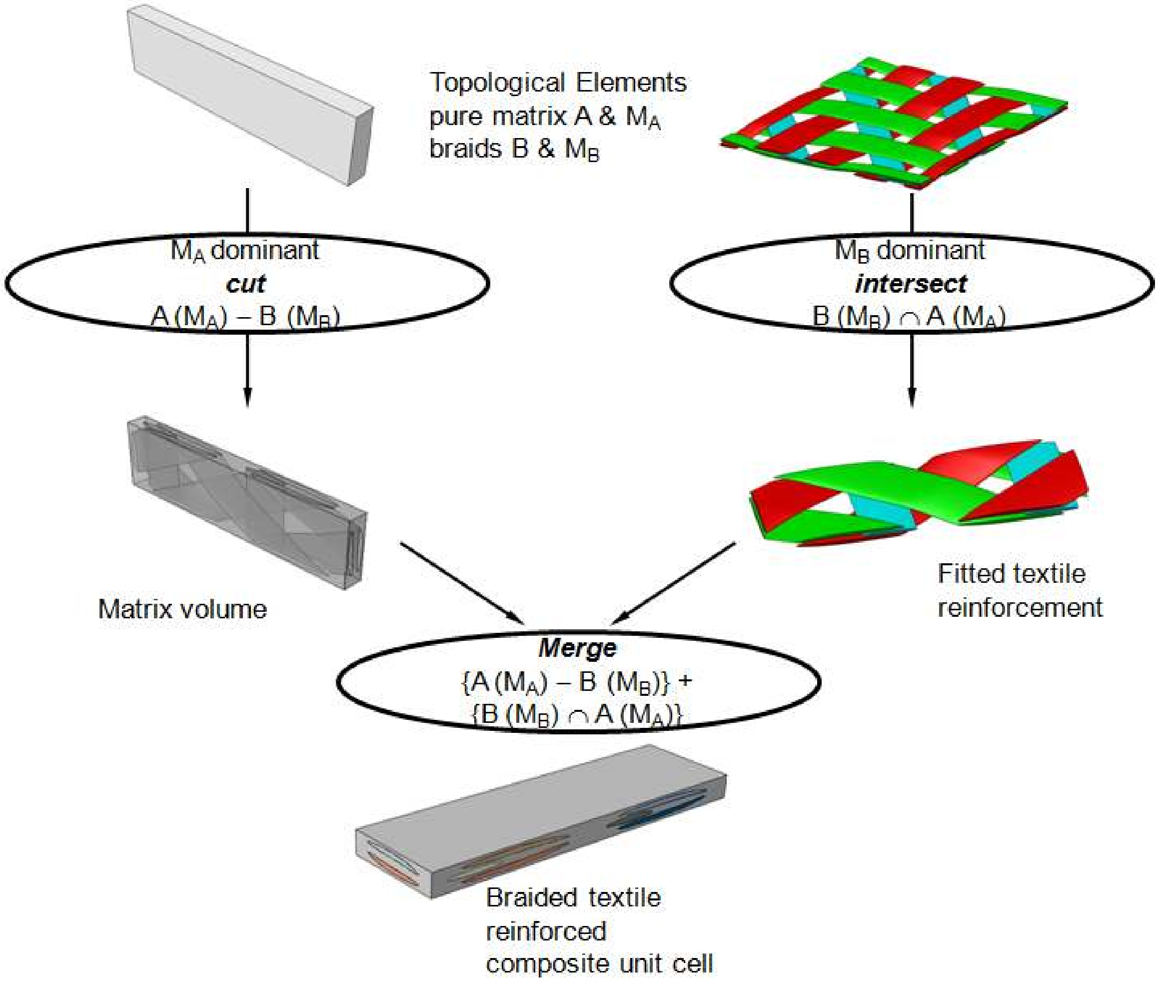


*Figure 5.Topology and procedures of constructing heterogeneous composite unit cell model*

## MATERIAL PROPERTIES AND ORIENTATIONS OF YARN

In this study, the matrix material is assumed to be isotropic and braiding yarns are assumed to be transversely isotropic. Since an impregnated braiding yarns consist of fibres and matrix, and each material has distinct properties; fibre volume fraction within yarn, $V_{fY}$, yarn volume fraction within a unit cell, $V_Y$, and global fibre volume fraction, $V_f$, are the important parameters to characterise the content of reinforcement in a composite. Their relation can be expressed as follows:

$$V_{fY} = \frac{V_f}{V_Y} \tag{2}$$

$V_{fY}$ is experimentally determined by the density method to be approximately 80%. This value will be used to calculate the equivalent mechanical properties of the braiding yarn on the basis of a micromechanical model, Chamis' Equations [16]:

$$E_{11} = V_{fY}E_{f11} + V_{mY}E_m \tag{3}$$

$$E_{22} = E_{33} = -\frac{E_m}{1-\sqrt{V_{fY}}(1-\frac{E_m}{E_{f22}})} \tag{4}$$

$$G_{12} = G_{13} = -\frac{G_m}{1-\sqrt{V_{fY}}(1-\frac{G_m}{G_{f12}})} \tag{5}$$

$$G_{23} = -\frac{G_m}{1-\sqrt{V_{fY}}(1-\frac{G_m}{G_{f23}})} \tag{6}$$

$$\nu_{12} = \nu_{13} = V_{fY}\nu_{f12} + V_{mY}\nu_m \tag{7}$$

$$\nu_{23} = \frac{E_{22}}{2G_{23}} - 1 \quad , \tag{8}$$

where $E_{11}$ is the longitudinal modulus of the yarns; $E_{22}$ and $E_{33}$ are the transversal moduli of the yarn; $G_{12}$, $G_{13}$, $G_{23}$ are the shear moduli of the yarn; $\nu_{12}$, $\nu_{13}$, $\nu_{23}$ are the Poisson's ratios of the yarn; $E_{f11}$ is the longitudinal modulus of the fibres; $E_{f22}$ and $E_{f33}$ are the transversal moduli of the fibres; $G_{f12}$, $G_{f13}$, $G_{f23}$ are the shear moduli of the fibres; $\nu_{f12}$, $\nu_{f13}$, $\nu_{f23}$ are the Poisson's ratios of the fibres; $E_m$ is the Yong's modulus of the matrix; $G_m$ is the shear modulus of the matrix; $\nu_m$ is the Poisson's ratio of the matrix; $V_{mY} = 1 - V_{fY}$ is the volume fraction of matrix in the yarn. $V_{fY}$ is set to be 0.8 based on experiments on carbon fibre textile composite coupons.

Due to the undulation of bias braiding yarns, the material orientation of every single yarn varies along its yarn path. Therefore, each bias yarn is segmented at the geometric modelling stage into several sub-cells, each of which is corresponded to a unique local coordinate system

(CSYS) to indicate the principle material orientation (see Figure 6). It should be noted that the whole unit cell is still subject to the global coordinate system.

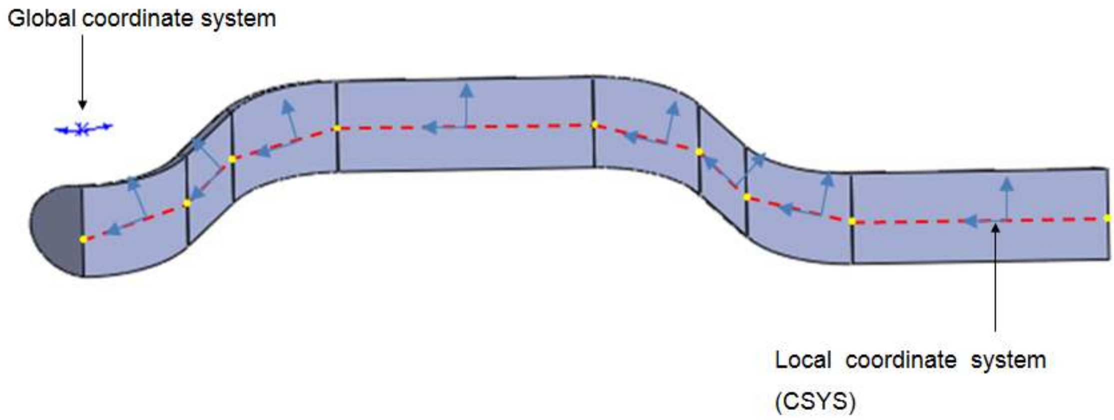


*Figure 6.Segmentation of individual bias yarns and local coordinate systems for sub-cell*

Table 1 summarises the material properties derived using Equations (3) to (8) and input for the FE-assisted unit cell simulations carried out in this study.

[Insert Table 1 here]

**BOUNDARY CONDITION AND MESH ISSUES**

As a unit cell is a small representative unit of a continuum braided textile composites, the periodicity of boundary conditions in FEA is of great concern. Xia et al. [19] devised a periodic boundary condition to match the deformation and mesh of neighbouring unit cells. For the unit cells studied in this paper, the periodic boundary condition and the minimisation of mesh mismatches is achieved through increasing the number of unit cells analysed in a single simulation while merging mismatched nodes on contacting faces. This method is computationally intensive, but the advantage lies in the relative ease of omitting user subroutines without compromising accuracy.

To obtain the material properties of the unit cell, seven independent boundary conditions in the form of uniform displacements are specified as shown in Figure 7. For each boundary condition, one corner point is held pinned to prevent rigid body motion.

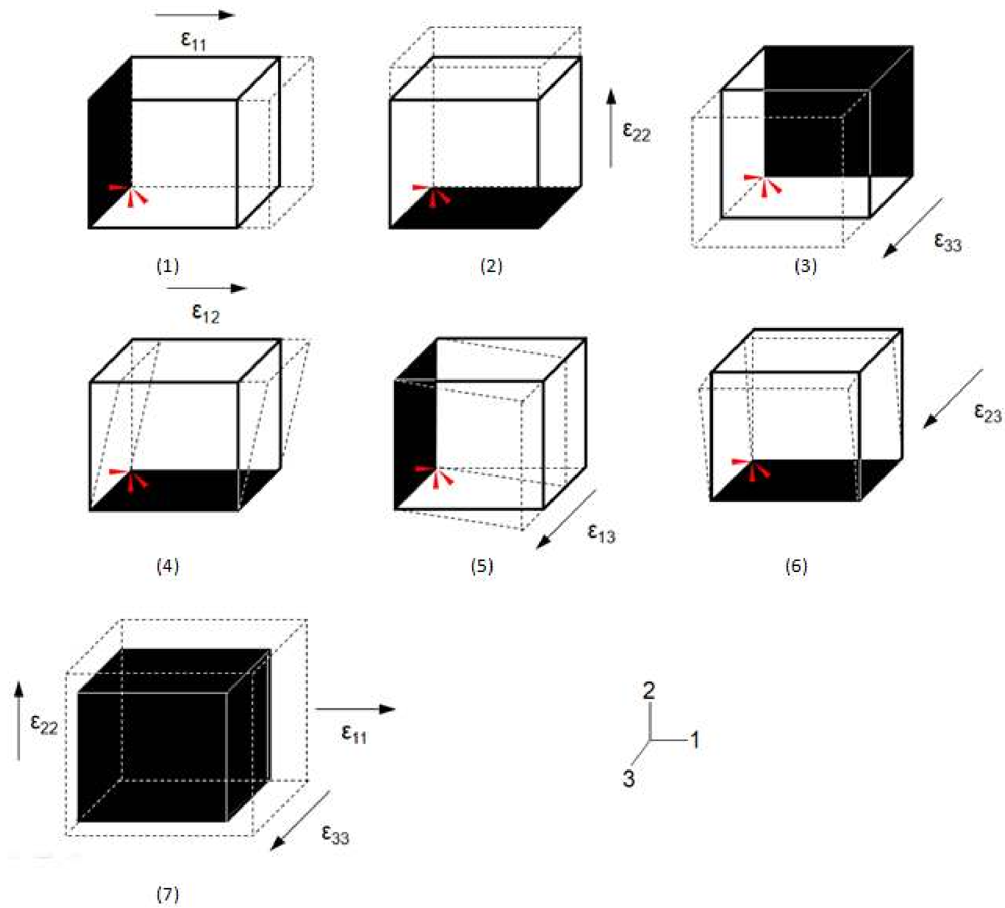


*Figure 7.Boundary conditions for finite element analyses*

The boundary conditions can be expressed mathematically as follows:

$$
\begin{aligned}
& u_1(0,y,z)=0 \\
& u_2(x,0,z)=0 \\
& u_3(x,y,0)=0 \\
& u_1(0,0,0)=u_2(0,0,0)=u_3(0,0,0)=0 \\
& u_1(l,y,z)-u_1(0,y,z)=\varepsilon_{11}\times[l,0,0]_1 \\
& u_2(x,w,z)-u_2(x,0,z)=\varepsilon_{22}\times[0,w,0]_2 \\
& u_3(x,y,t)-u_3(x,y,0)=\varepsilon_{33}\times[0,0,t]_3 \\
& u_2(l,y,z)-u_2(0,y,z)=\gamma_{12}\times[l,0,0]_1 \\
& u_2(x,y,t)-u_2(x,y,0)=\gamma_{23}\times[0,0,t]_3 \\
& u_1(x,y,t)-u_1(x,y,0)=\gamma_{31}\times[0,0,t]_3
\end{aligned} \tag{9}
$$

where, $u_1$, $u_2$ and $u_3$ are uniform displacement applied in the x, y and z directions, respectively, and l, w, and t denote the length, width, and thickness of the unit cell model. A more general form can be found in [11]. To obtain homogenised Young's moduli and shear moduli of the unit cell, mean stress, $\overline{\sigma}$ , is calculated for relevant boundary condition case by dividing the summation of the reaction forces of all the nodes on the face, where the displacement boundary condition is applied to, by the area of that displaced face. Whereas, mean strain, $\overline{\varepsilon}$ , is defined when assigning boundary conditions. A component form of linear stress-strain relation for braided textile composite unit cell, $\overline{\sigma}=\overline{C}\,\overline{\varepsilon}$ , can be formulated as follows:

$$
\begin{pmatrix} \overline{\sigma_{11}} \\ \overline{\sigma_{22}} \\ \overline{\sigma_{33}} \\ \overline{\sigma_{44}} \\ \overline{\sigma_{55}} \\ \overline{\sigma_{66}} \end{pmatrix} = \begin{bmatrix} \overline{C_{11}} & \overline{C_{12}} & \overline{C_{13}} & 0 & 0 & 0 \\ \overline{C_{21}} & \overline{C_{22}} & \overline{C_{23}} & 0 & 0 & 0 \\ \overline{C_{31}} & \overline{C_{32}} & \overline{C_{33}} & 0 & 0 & 0 \\ 0 & 0 & 0 & \overline{C_{44}} & 0 & 0 \\ 0 & 0 & 0 & 0 & \overline{C_{55}} & 0 \\ 0 & 0 & 0 & 0 & 0 & \overline{C_{66}} \end{bmatrix} \begin{pmatrix} \overline{\varepsilon_{11}} \\ \overline{\varepsilon_{22}} \\ \overline{\varepsilon_{33}} \\ \overline{\varepsilon_{44}} \\ \overline{\varepsilon_{55}} \\ \overline{\varepsilon_{66}} \end{pmatrix} \tag{10}
$$

Inverting the stiffness matrix $\overline{C}$ gives the compliance matrix $\overline{S}$ . Given the mean stress vector and mean strain vector inputs obtained from each boundary condition cases, the equivalent engineering constants can be computed from the constituent entities of the compliance matrix. With respect to the Poisson's ratios, two rounds of simulation are conducted. The first round of simulation consists of three unidirectional deformations (cases 1-3 in Figure 7) to obtain $E_{11}$, $E_{22}$ and $E_{33}$ individually and their values are supposed to be boundary-condition-independent; the second round of simulation involves a triaxial deformation (case 7 in Figure 7) to extract three mean stress values, $\sigma_{11}$, $\sigma_{22}$, and $\sigma_{33}$ under triaxial loading. All this six parameters are subsequently input into the stiffness matrix to compute the value of Poisson's ratios.

## RESULTS AND DISCUSSION

Intuitively, the relation between elastic properties and the braiding angle should be symmetrical about θ=45° if everything else being identical, since the longitudinal Young's modulus of a unit cell with braiding angle (θ) would equal the transverse Young's modulus of another unit cell with braiding angle (90-θ). However, this symmetry will not be observed because the unit cells studied in this paper are governed by Equation (1) which links the braiding angle with tightness of a unit cell. As the braiding angle increases, the unit cell becomes tighter. As such, by rotating a (θ) unit cell will not give a (90-θ) unit cell due to the tightness difference. Figure 8 illustrates how the braiding angles determine the geometries of the braided textile composite unit cells for θ=20°, 40° and 60°.

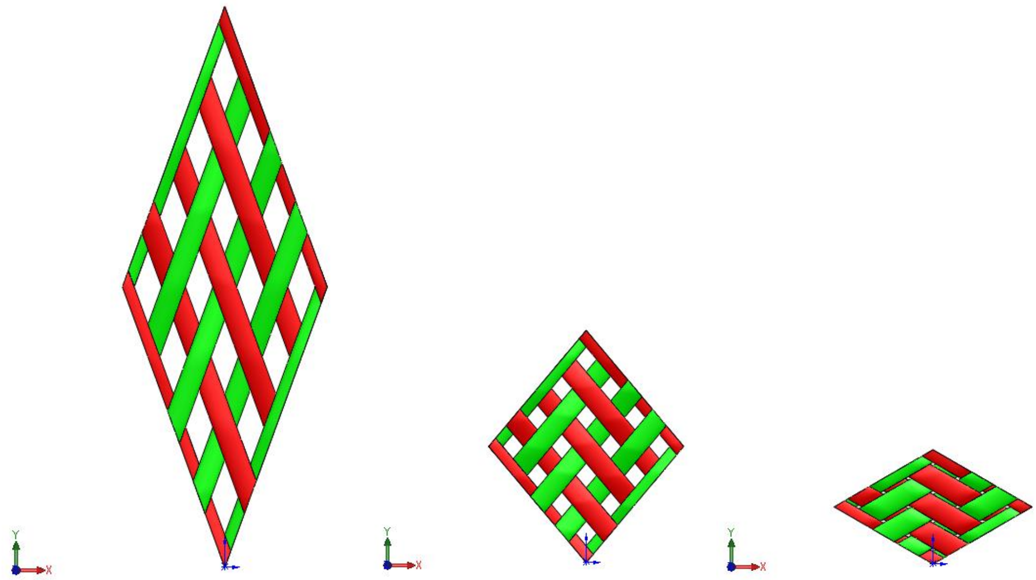

*(a) θ=20°* *(b) θ=40°* *(c) θ=60°*

*Figure 8.The effect of braiding angles on the tightness of braid unit cells*

The stress distributions of rectangular unit cells with braiding angles 30° and 40° are presented in Figure 9 under transverse tensile boundary conditions. It is clearly observed that stress concentration mainly occurs along the edges of the yarn, agreeing with [12].

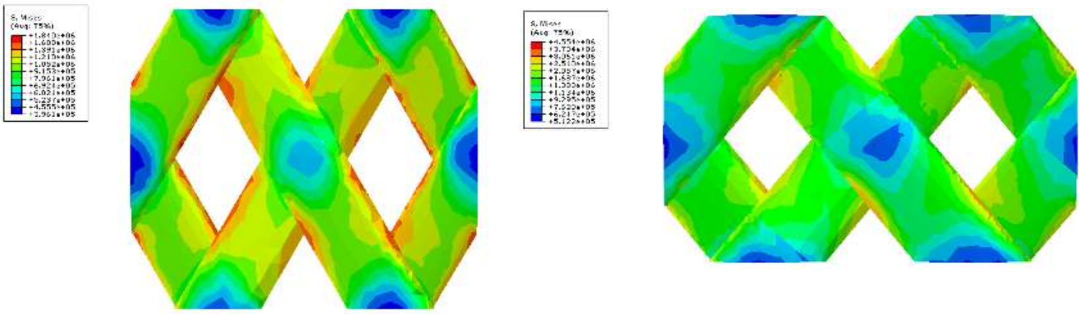

*Figure 9. Stress distribution within braiding yarns under tensile loading along transverse directions for braiding angles 30° (left) and 40° (right)*

As described earlier, a multi-cell approach is used to represent the periodic boundary conditions. If the contour distribution of the multi-cell model can be recognised as a repetition of that of the corresponding single unit cell model, the proposed approach is then proved to be valid. A comparison of multi and single unit cell models for regular biaxial braids under in-plane shear displacement is shown in Figure 10. It can be seen that the stress distribution of the multi-cell (4×4) model agrees with that of the corresponding single unit cell model, and the maximum and minimum stresses are almost identical. Other boundary conditions are verified in the same way.

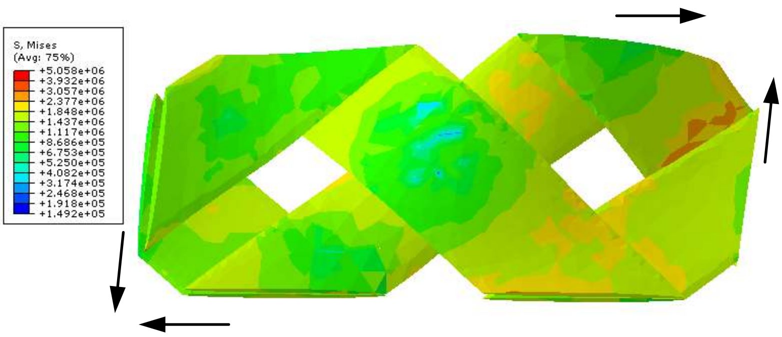

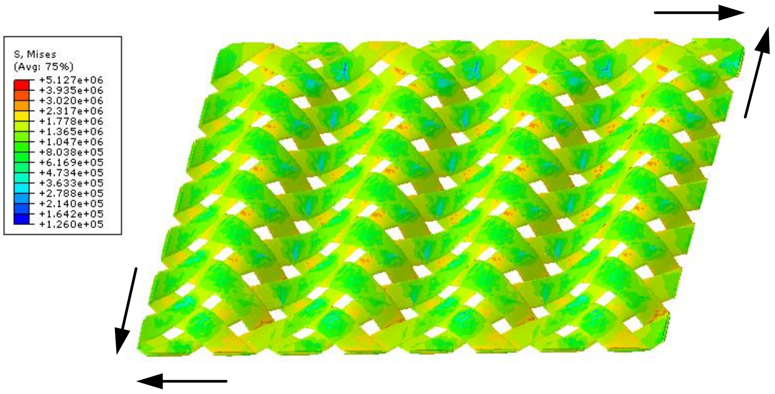


*Figure 10. Comparison of stress distribution in multi-cell and single unit cell under in-plane shear deformations for braiding angle 50°*

**The Effect of Braiding Angle on Mechanical Properties**

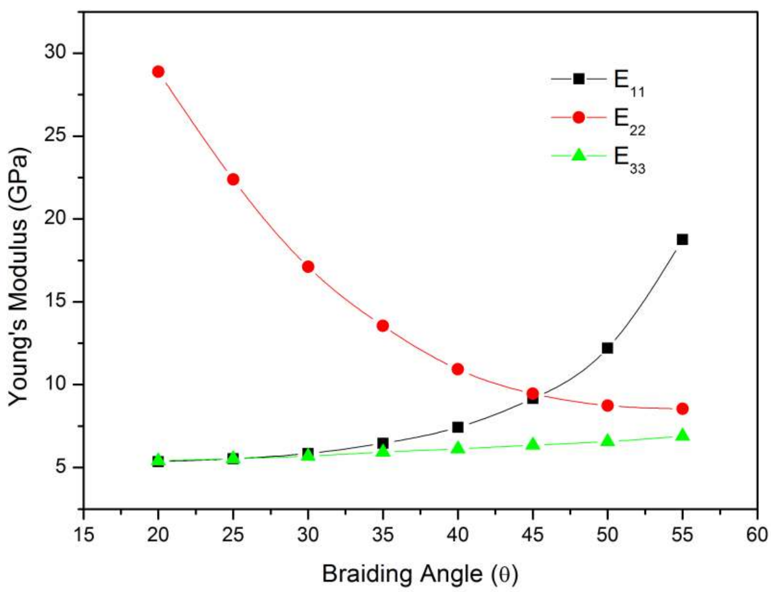


*Figure 11.The effect of braiding angle on the Young’s moduli for biaxial unit cell*

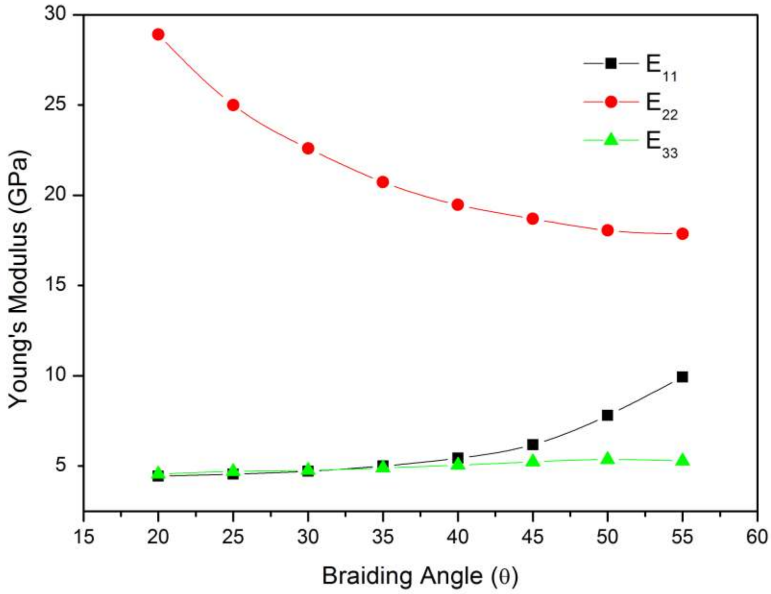


*Figure 12.The effect of braiding angle on the Young's moduli for triaxial unit cell*

As depicted in Figure 11, for biaxial unit cells, the longitudinal Young's modulus, $E_{22}$, decreases with the increase of braiding angle; whereas, the transverse Young's modulus, $E_{11}$, increases with the braiding angle θ. This is because braiding yarns contribute more to transverse discretion and less to longitudinal direction as braiding angle increases. However, the Young's modulus in through-thickness-direction, $E_{33}$, only increases slightly and this increase is mainly due to the increase in tightness. Shown in Figure 12, the relation between Young's moduli and braiding angle for triaxial unit cell exhibits a similar trend. The main difference is that, due to the presence of axial yarns, the value of longitudinal Young's modulus $E_{22}$ is always greater than the value of transverse Young's modulus $E_{11}$. The differences accurately explain the reinforcing effect of axial yarns.

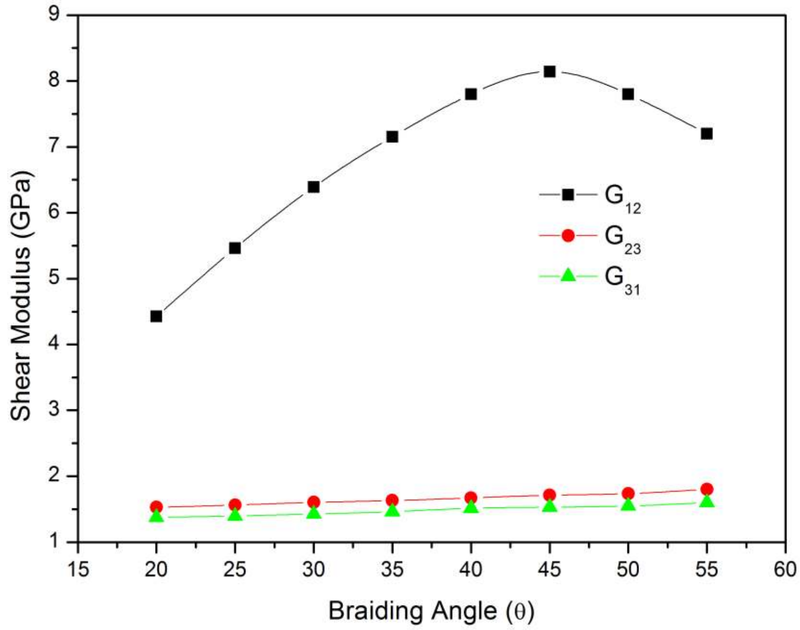


*Figure 13.The effect of braiding angle on the shear moduli for biaxial unit cell*

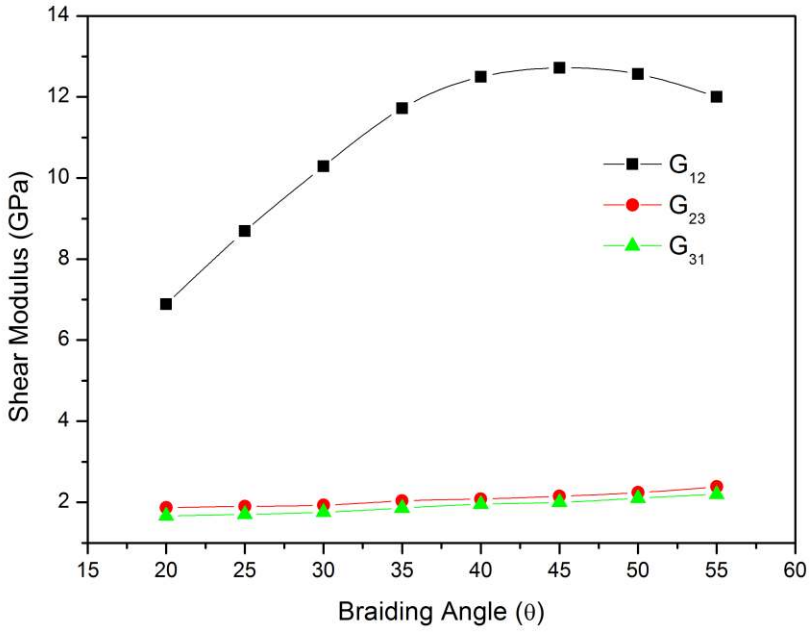


*Figure 14.The effect of braiding angle on the shear moduli for triaxial unit cell*

The relations between shear moduli and braiding angle for biaxial and triaxial structures are depicted in Figure 13 and Figure 14, respectively. The in-plane shear modulus, $G_{12}$, increases with the braiding angle and peaks at the braiding angle of 45°. It means that woven structure (θ=45°) enjoys higher in-plane shear rigidity than their braided counterparts. However, the through-thickness-shear moduli, $G_{23}$ and $G_{13}$, increase insignificantly with the increase of braiding angle. Similarly, this can be explained by the tightness variations.

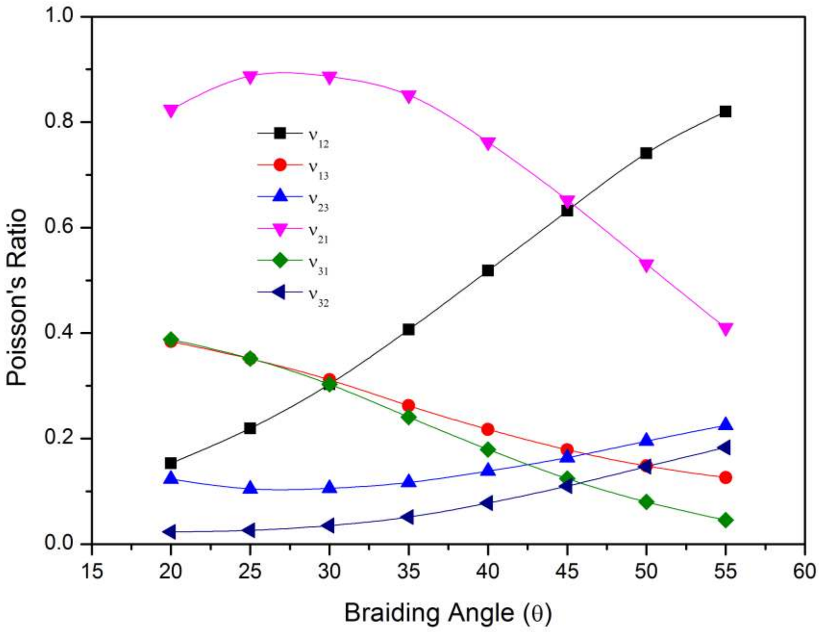


*Figure 15.The effect of braiding angle on the Poisson's ratio for biaxial unit cell*

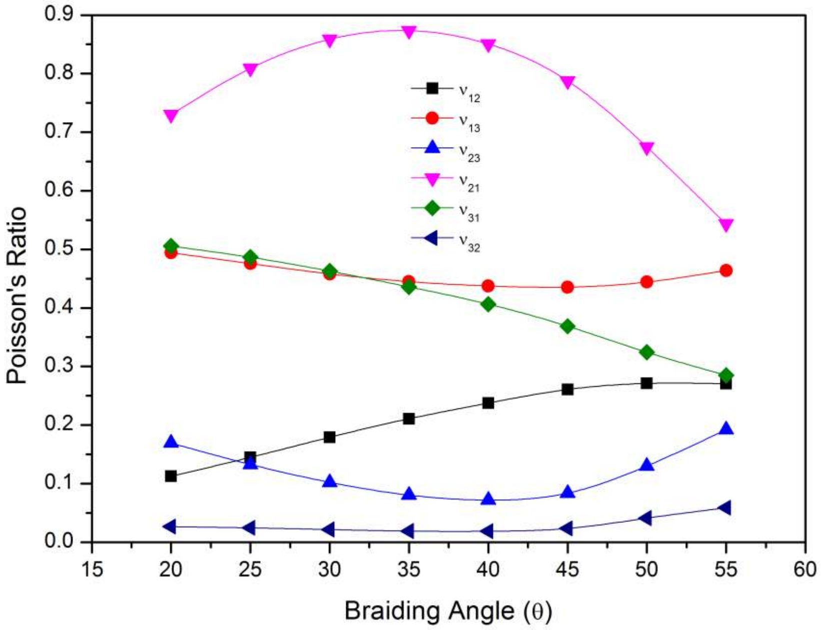


*Figure 16.The effect of braiding angle on the Poisson's ratio for triaxial unit cell*

As delineated in Figure 15 and Figure 16, all the Poisson's ratios vary in a nonlinear manner with the increase of braiding angle. Specifically, the in-plane Poisson's ratio, $\nu_{21}$, is significantly higher than all the other Poisson's ratios, especially at low braiding angles; contrarily, the Poisson's ratio, $\nu_{32}$, in through-thickness-direction is generally lower than the rest. Unlike the traditional isotropic materials which Poisson's ratio range is between 0.35 and 0.5, some of the Poisson's ratios of braided textile composite have values that are close to 1. In general, for anisotropic materials including fibrous and textile reinforced composites, the value of Poisson's ratio depend on direction. Poisson's ratios are reported to have large magnitudes of positive [20] or negative [10] values. In the specific context of braided textile composite of this paper, the reason lies in the fact that great disparity in terms of moduli in longitudinal and transverse directions of constituent braiding yarns and the resultant significantly dissimilar reinforcing effects of the braided textile preform along different directions lead to a high anisotropy of composite material property. For example, a combination of high Young's modulus in the longitudinal direction and low modulus in the transverse direction will lead to a high value of minor Poisson’s ratio. It is also noticed that at angle of 45°, $\nu_{21} = \nu_{12}$, $\nu_{23} = \nu_{32}$, $\nu_{13} = \nu_{31}$. This is due to the unit cell having identical properties in both planar directions at angle of 45°.

**The Effect of Fibre Volume Fraction on The Mechanical Properties**

For a typical braided structure, $V_f$ can reach 0.5 to 0.6 because of tight braiding architectures as a result of net-shape-manufacture technique [11]. In this study, $V_f$ is controlled by the thickness of the unit cell. Its range of 0.40 to 0.55 guarantees the practical usefulness of the FE model and the results.

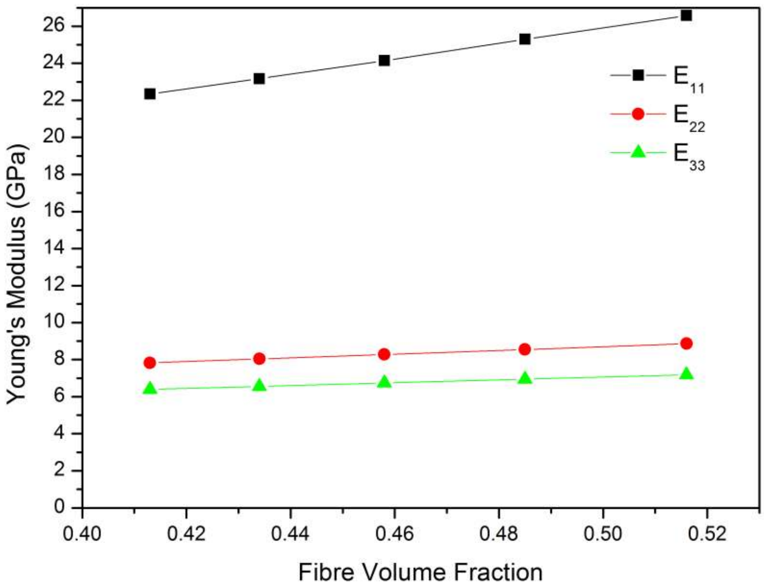


*Figure 17.The effect of fibre volume fraction on the Young’s moduli for biaxial unit cell*

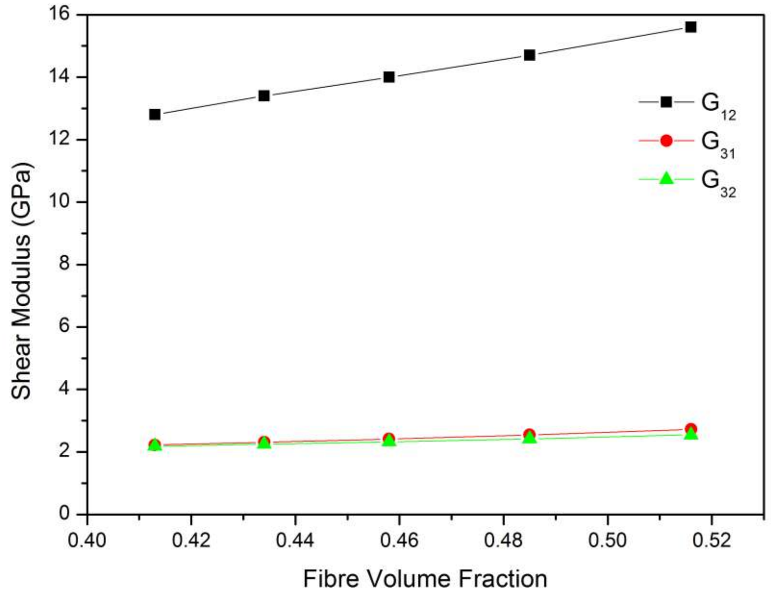


*Figure 18.The effect of fibre volume fraction on the shear moduli for biaxial unit cell*

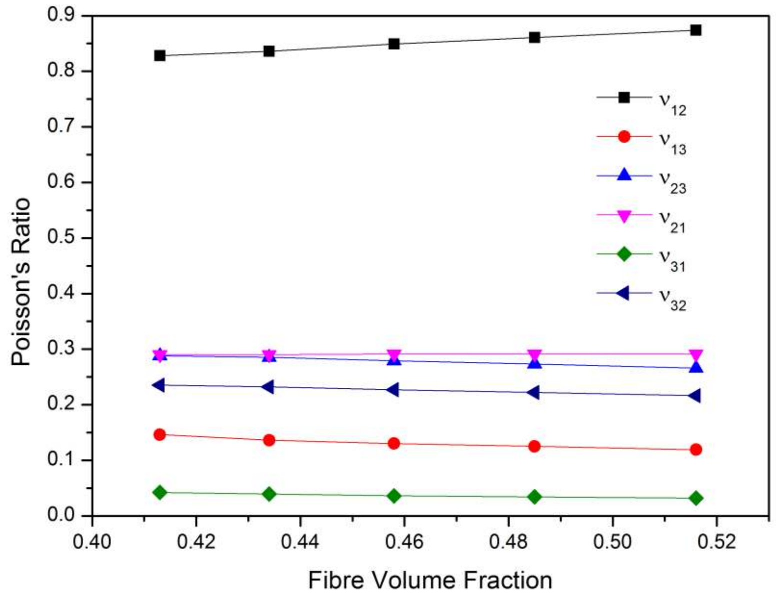


*Figure 19.The effect of fibre volume fraction on the Poisson's ratios for biaxial unit cell*

The effect of $V_f$ on the equivalent mechanical properties is investigated for unit cells with a fixed braiding angle of 60°. As depicted in Figure 17, the Young's moduli correlate with $V_f$ linearly. Similarly, as shown in Figure 18, all the shear moduli, $G_{12}$, $G_{13}$, and $G_{23}$, increase linearly with the increase of $V_f$, and the in-plane shear modulus, $G_{12}$, increases more as compared to the two through-thickness shear moduli.

As delineated in Figure 19, the in-plane Poisson's ratio, $\nu_{12}$, is noticeably higher than all the other Poisson's ratios. The explanation is that the high braiding angle leads to more yarns to lean towards the transverse direction. The value of $\nu_{12}$ increases with the increase of $V_f$, and $\nu_{21}$ almost remains constant with the increase of $V_f$. In contrast, the other four Poisson's ratios, $\nu_{31}$, $\nu_{32}$, $\nu_{23}$ and $\nu_{13}$, tend to have an inverse relation with $V_f$. The linearity demonstrated by the relations between elastic properties and $V_f$ indicates that the general principle of rule of mixture, which primarily applies to unidirectional fibre laminates, can also be extrapolated to study braided textile composites. However, $M^{Textile}_{Equivalent}$ in Equations (11) and (12) refers to the equivalent property of reinforcing braided textile in its composite instead of it consisting of individual dry yarns.

$$M^{Composite}_{In-plane} = M^{Textile}_{Equivalent} V_f^{Textile} + M^{Matrix}(1 - V_f^{Textile}) \quad (11)$$

$$\frac{1}{M^{Composite}_{In-plane}} = \frac{V_f^{Textile}}{M^{Textile}_{Equivalent}} + \frac{1 - V_f^{Textile}}{M^{Matrix}} \quad (12)$$

## VERIFICATION OF SIMULATION RESULTS BY A BENDING TEST

### Bending Test Set-Up

The bending test is a basic mechanical test which provides information on the modulus of elasticity in bending $E_f$ and the flexural stress-strain response of the material. A beam structure which has variable braid angles through the cross-section was intentionally chosen in this study. Geometrically, this structure consisted of a rounded leading edge, a sharp trailing edge and an asymmetric camber. The beam, which structure consists of foam core enveloped by composite skin comprising 2 layers of 2x2 biaxial reinforcement braids, was fabricated using Resoltech

2080 M25 foam core and Aksaca carbon fibre braided textile composite skin by wet-layup fabrication process.

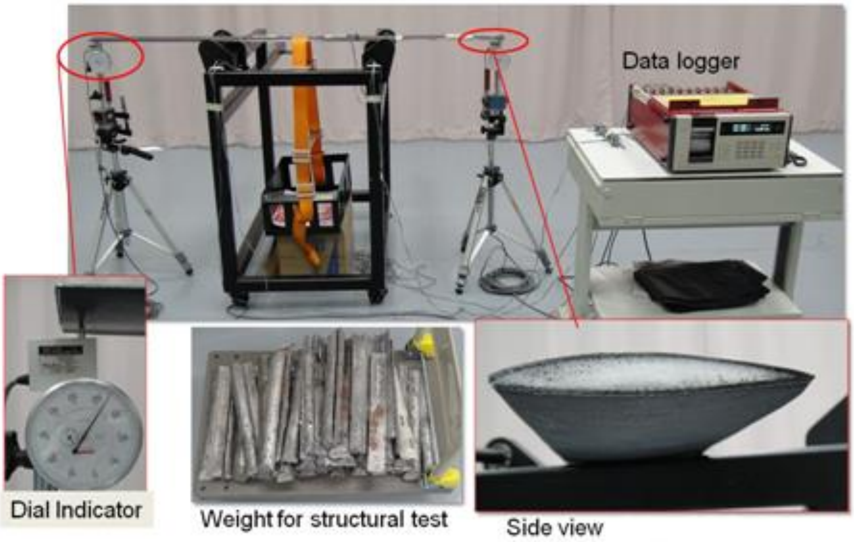


*Figure 20.Beam design and experimental setup*

Loaded in the three-point configuration, the actual test set-up of the beam structures is shown in Figure 20 where the assembly was supported by two rods. In contrast to conventional three point bending test, the bending force was applied via belt loading where loads were increased progressively. Two strain gauges were installed at the bottom to measure the tensile strain values. The strain was measured and recorded by a portable data logger TDS-302 while the tip deflections were measured by two dial indicators DDP-50A. Both sets of equipment were manufactured by Tokyo Sokki Kenkyujo Co., Ltd. The contact area that applies the belt load is shaded yellow and the locations of strain gauge applied are shown in Figure 21. The strain gauges are shown by the blue rectangles just offset from the central contact area and the contact area consists of the curved top surface with a width of 50 mm and a length of 142 mm at the centre of the beam.

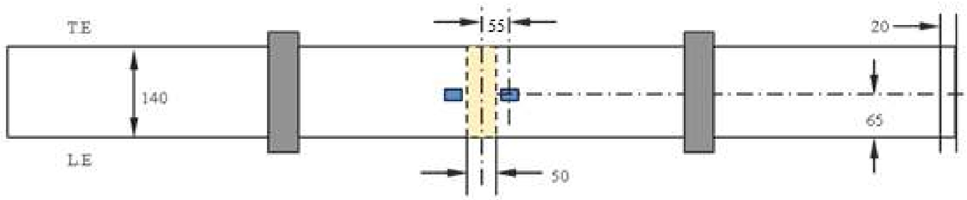


*Figure 21. Locations of strain gauges and the area that applies the load*

**Yarn and Foam Core Properties**

Aksaca carbon fibre was produced by De Long & Associates LLC with polymer system supplied by Momentive Specialty Chemicals, and the properties of the impregnated braiding tows were determined by Equations (3) to (8). The properties were $E_{11} = 193.7$ GPa, $E_{22} = E_{33} = 11.8$ GPa, $\nu_{12} = \nu_{13} = 0.23$, $\nu_{23} = 0.25$, $G_{12} = G_{31} = 8.43$ GPa, and $G_{23} = 4.71$ GPa. Resoltech 2080 M25 is a typical liquid foaming epoxy, mixed with Hardener 2085M on a weight ratio 100:30, to cast low density structural cores. It was treated as an isotropic material with elastic material properties: E = 213 MPa, G = 98 MPa.

**Unit Cell Discretisation and Meso-Level Simulation**

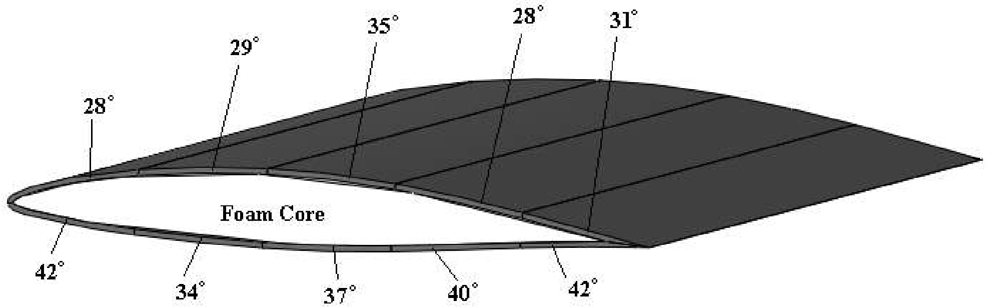


*Figure 22.Discretisation of beam structure based on braiding angle*

In this analysis, each surface (top and bottom) of the composite skin was subdivided into five sections along its chord length (see Figure 22). For top surface unit cells, braiding angles vary from 28° to 35° while bottom ones have braiding angles from 34° to 42°. This variation is mainly due to changing curvature of the beam profile. But we also anticipate and deliberately carry this out to account for imperfection and uncertainties inherent in the real-world fabrication process.

All these unit cells were modelled individually with yarn widths of 3 mm, thicknesses of 0.2875 mm and inter-yarn spacing, ε, of 0.05 mm. The composite skin thickness is maintained at 1.3 mm (two layers of braided textile reinforcements). Each unit cell construction was optimized to ensure non-conflicting yarns due to the tight textile spatial constraints, details see [21]. Determined by FEA on unit cell, the elastic properties of the unit cell with the braiding angle of 28° from the top surface were determined to be $E_{11}$ = 11.7GPa, $E_{22}$ = 43.6GPa, $E_{33}$ = 9.41GPa, $\nu_{12}$ = 0.254, $\nu_{13}$ = 0.233, $\nu_{23}$ = 0.104, $G_{12}$ = 20.9GPa, $G_{31}$ = 3.39GPa, and $G_{23}$ = 4.26GPa. By the same procedure, the elastic constant values for the remaining sections on the top surface and all sections of the bottom surface were obtained uniquely.

**Macro Level Bending Simulation on the Beam**

Having obtained the elastic properties of the ten sections on the beam structure, a macro level simulation of the loaded structure could be carried out.

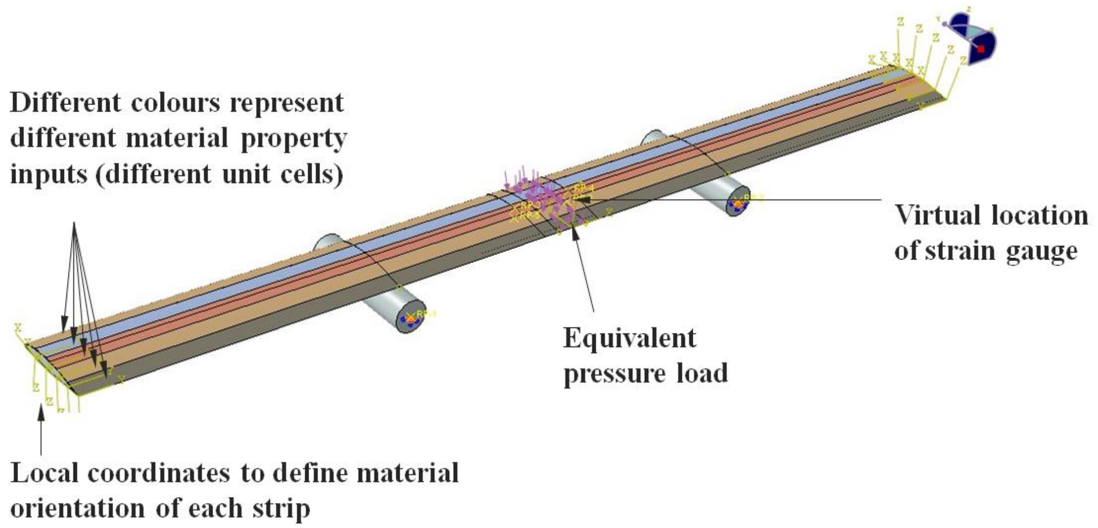


*Figure 23.Beam subsection properties and orientations*

As depicted in Figure 23, each partition of the beam structure was assigned the unit cell elastic mechanical properties corresponding to their braiding angles. Ten local coordinates perpendicular to the curvature of the top and bottom surfaces of each section were assigned to define the material orientation. In the meshes, 3D hexagon 8-node C3D8R elements were used for the majority of all the constituents with some small regions being meshed with linear wedge elements of type C3D6. There were 55641 nodes in total. The central region of the beam experiences a constant pressure load similar to that applied in the actual experiment.

The supporting rods (which were created and assembled with the beam in Abaqus) were assumed to be rigid bodies supporting the beam structure throughout the analysis. Partitions were also made on the beam to isolate the regions of the applied load and the other points of interest (i.e., strain gauge locations, contact points of the supporting rods, etc.). The contact between supporting rods and the beam was assumed to be frictionless. The translational movement in Y direction and rotational degree of freedoms in X and Z directions of the two contact points were constrained (U2=UR1=UR3=0) in order to provide optimal constraints to the loaded structure. At the same time, they are also the minimal constraint; any lesser constraint will lead to either asymmetrical deformation or convergence problems in the simulation.

**Results and Discussion**

The contour plot of the maximum principal stress (Figure 24) shows the stress concentrations occur at the centre of the beam structure, which is expected due to the applied load and the constraining boundary conditions. The discontinuity in the stress distribution is the result of the discretization process and can be mitigated by increasing the density of discretization. And as shown in Figure 25, the simulated strain value lies in between the strain value measured by the left and right strain gauges. Generally, there is a good correlation between the experimental measurements and the FEA predictions of strain.

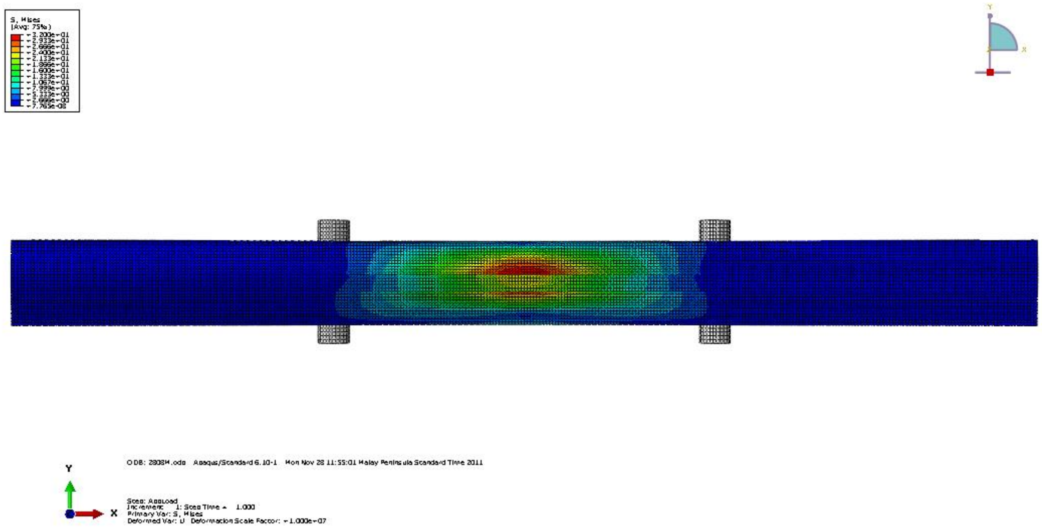

*Figure 24.Contour plot of maximum principal stress (top view)*

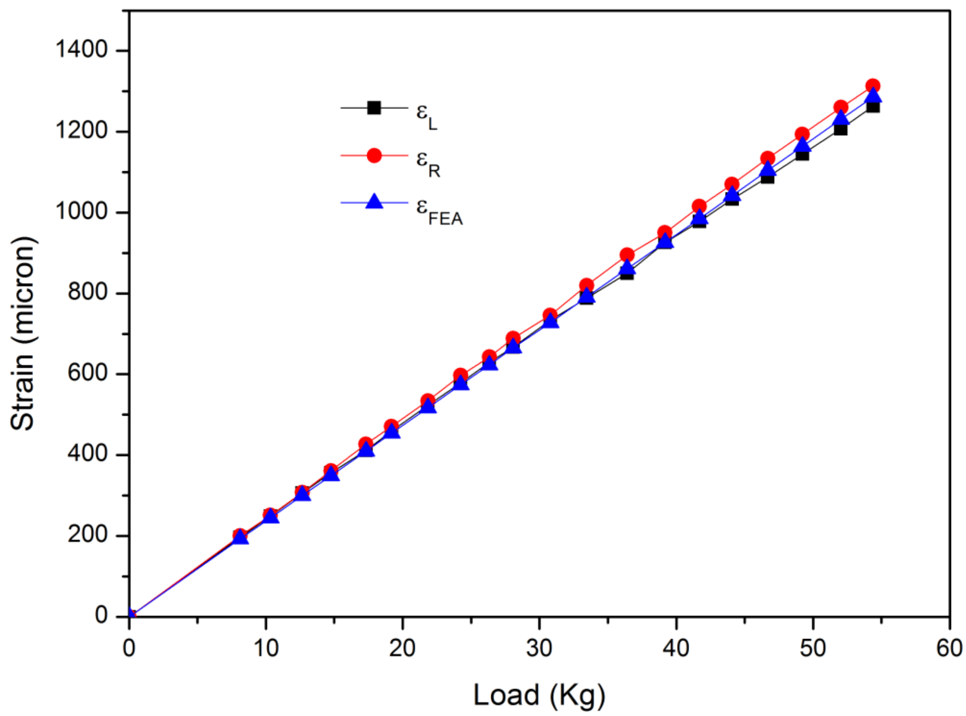


*Figure 25.Correlation of simulated and tested strain value*

Another measure of comparison is the tip displacement experienced by the structure. One deformed shape of the beam at an applied load is shown in Figure 26. The agreement between simulated displacement and actual displacement is very good as shown in Figure 27.

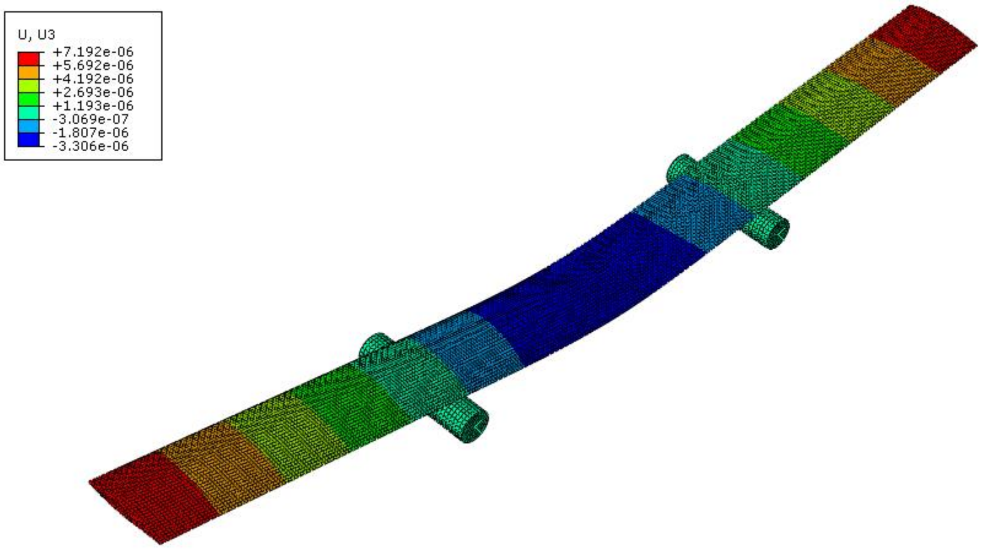


*Figure 26.Beam tips displacement*

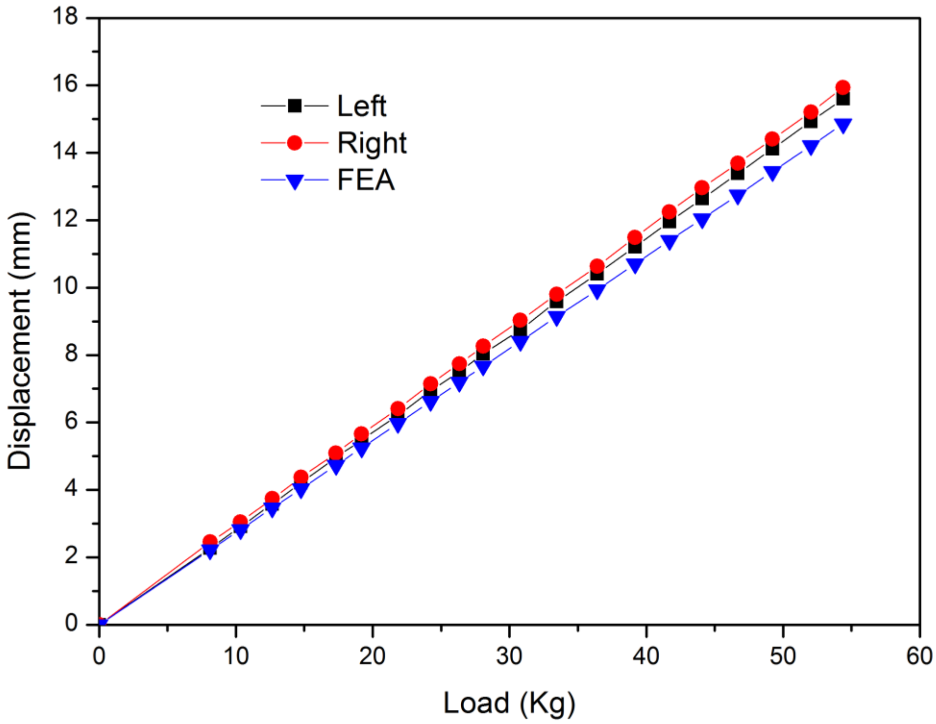


*Figure 27.Correlation of simulated and tested beam tip displacement value*

These two positive correlations of the FEA with the experiments at not only within the interior of the structure (where the strain gauges lie) but also at the boundaries (tips) exhibit an overall agreement in the predicted and the actual elastic behaviour of the structure. The minor divergence in strain and displacement values with the increase of load can be explained by a few factors. Notice that a single value of elasticity was adopted in this study according to data provided by the supplier, while it was fully acknowledged that the tensile elasticity may deviates from compression modulus for porous foam materials; this approximation was a possible source of discrepancy between simulation and experimental results. Moreover, the resin matrix, epoxy, is a brittle material in which micro cracks can propagate easily once initiated under load. In contrast, FEA treats the body as a perfect material, ignoring the possible defects in the structure. Therefore, it was likely that the structure's stiffness degraded slightly below the values predicted using the unit cell modelling as the load increased. Additionally, the number of discretization of the beam structure (currently 10 sections) may affect the prediction as well. More regions would lead to better region-wise property determination and a more accurate elastic behaviour simulation. Adding more partitions in regions of particularly high curvature (and changing braid angles) might also lead to better results as well. However, the computation cost will increase, thus there is always a trade-off between simulation efficiency and simulation accuracy.

## CONCLUSIONS

In this paper, geometric and finite element models of 2D biaxial and triaxial braided textile preform and their composite unit cells are systematically developed and analysed. The unit cells proposed in this work are highly dynamic and versatile and able to resemble different jamming conditions [22]. The variations of elastic mechanical properties of braided composites with the increase of braiding angle presented show an expected asymmetry about θ=45°, mainly due to the additional constraint of yarn spacing being dependent on braiding angle. It is also found that all the in-plane engineering constants are more sensitive to the braiding parameters than the properties involve the through-thickness direction. Additionally, it is demonstrated that there exist a linear correlation between fibre volume fraction and the elasticity constants for a given braiding angle, and this linearity can be harnessed as a rule of thumb to estimate the properties of composites with different fibre volume fractions. Acknowledging the shortcomings of small scale coupon testing, another uniqueness of this paper lies in the direct comparison between a bending test on a composite structure and FEA obtained via the multi-scale modelling approach. The proposed model is shown to be able to predict the mechanical behaviour of braided composites accurately and efficiently.

**ACKNOWLEDGEMENT**

Financial support from Defence Science and Technology Agency (DSTA) of Singapore is gratefully acknowledged.

**Reference**

[1]Lee S.M. (1993). *Handbook of composite reinforcements*. Weinheim: Wiley-VCH.

[2] Carbonfibreguru.com. Available at http://www.carbonfiberguru.com/

[3]Naik N.K. and Shembekar P.S. (1992). Elastic Behavior of Woven Fabric Composites: I—Lamina Analysis, *Journal of Composite Materials*, **26**: 2196-2225.

[4]Quek S.C., Wass A.M., Shahwan K.W. and Agaram V. (2003). Analysis of 2D triaxial flat braided textile composites, *International Journal of Mechanical Science*, **45**: 1077–1096.

[5]Miravete A., Bielsa J.M., Chiminelli A., Cuartero J., Serrano S., Tolosana N. and Guzman de Villoria R. (2006). 3D mesomechanical analysis of three-axial braided composite materials, *Composite Science and Technology*, **66**: 2954-2964.

[6]Falzon P.J. and Herszberg I. (1998). Mechanical performance of 2-D braided carbon/epoxy composites, *Composite Science and Technology*, **58**: 253–265.

[7]Dauda B., Oyadiji S.O. and Potluri P. (2009). Characterising Mechanical Properties of Braided and Woven Textile Composite Beams, *Applied Composite Materials*, **16**:15–31.

[8]Littell J.D., Binienda W.K., Roberts G.D. and Goldberg R.K. (2009). Characterization of Damage in Triaxial Braided Composites under Tensile Loading, *Journal of Aerospace Engineering*, **22**(3): 270-279

[9]Masters J.E., Foye R.L., Pastore C.M. and Gowayed Y.A. (1993). Mechanical properties of triaxially braided composites: experimental and analytical results, *Journal of Composites Technology and Research*, **15**: 112–22.

[10]Tsai K.H., Hwan C.L., Chen W.L. and Chiu C.H. (2008). A parallelogram spring model for predicting the effective elastic properties of 2D braided composites, *Composite Structure*, **83**: 273–283.

[11]Xu L., Kim S.J., Ong C.H. and Ha S.K. (2012). Prediction of material properties of biaxial and triaxial braided textile composites, *Journal of Composite Materials*, **0**:1-16.

[12]Goyal D. and Whitcomb J.D. (2006). Analysis of Stress Concentrations in 2×2 Braided Composites, *Journal of Composite Materials*, **40**: 533-546.

[13]Pickett A.K., Sirtautas J. and Erber A. (2009). Braiding Simulation and Prediction of Mechanical Properties, *Applied Composite Materials*, **16**:345–364.

[14]Chia S.M., Tan Y.C., George W.D. and Frank K.K. (2004). A dynamic unit cell model for design & analysis of 2-D braided structures, In: *7$^{th}$ International Conference on Textile Composites*, Japan.

[15]Sun W., Lin F. and Hu X. (2000). Computer-aided design and modeling of composite unit cells, *Composite Science and Technology*, **61**: 289-299.

[16]Chamis C.C. (1989). Mechanics of Composite Materials: Past, Present and Future, *Journal of Composites Technology and Research*, **11**(1): 3–14.

[17]Tate J. (2004). Performance Evaluation and Modeling of Braided Composites, PhD Dissertation, North Carolina A&T University.

[18]Tsai S.W. and Hahn H.T. (1980). Introduction to composite materials, Lancaster: Technomic Publishing.

[19]Xia Z., Zhang Y. and Ellyin F. (2003). A unified periodical boundary conditions for representative volume elements of composites and applications, *International Journal of Solids Structures*, **40**:1907-1921.

[20] Tate J., Kelkar A. and Whitcomb J. (2006). Effect of braid angle on fatigue performance of biaxial braided composites, *International Journal of Fatigue*, **28**: 1239–1247.

[21]Ji X., Khatri A.M., Chia S.M., Cha K.H., Yeo T.B., Joshi S. and Chen Z. (2012) Multi-scale modeling of variable angle braided textile composites and its validation, In: *1st Brazilian Conference on Composite Materials (BCCM1)*, Natal-RN.

[22] Khatri A.M., Ji X., Joshi S. and Chen Z. (2011) Textile tightening simulation in regular braided textile composites using dynamic unit cell models, In: *International Conference on Materials for Advanced Technologies (ICMAT) 2011*, Singapore.

Table 1.Material properties of fibre [17], matrix [18] and yarn

| Material properties | Fibre | Material properties | Matrix | $V_{fY}$ | Material properties | Yarn |
|---|---|---|---|---|---|---|
| $E_{f11}$ (GPa) | 227.53 | $E_m$ | 3.45 GPa | 0.8 | $E_{11}$ (GPa) | 182.71 |
| $E_{f22}$=$E_{f33}$ (GPa) | 16.55 | $N_m$ | 0.35 | | $E_{22}$=$E_{33}$ (GPa) | 11.81 |
| $G_{f12}$=$G_{f13}$ (GPa) | 24.82 | | | | $G_{12}$=$G_{13}$ (GPa) | 8.43 |
| $G_{f23}$ (GPa) | 6.89 | | | | $G_{23}$ (GPa) | 4.71 |
| $\nu_{f12}$= $\nu_{f13}$ | 0.20 | | | | $\nu_{12}$=$\nu_{13}$ | 0.23 |
| $\nu_{f23}$ | 0.25 | | | | $\nu_{23}$ | 0.25 |